DIELECTRIC PROPERTIES OF $Y_{2/3}Cu_{3-x}Zn_xTi_4O_{12}$ (x = 0.10, 0.20 and 0.30) SYNTHESIZED BY SEMI-WET ROUTE

CHAPTE

5

5.1 INTRODUCTION

The applications of high dielectric constant materials are in focus, not only for purely academic reasons but also for the further development of modern electronics. A high dielectric constant material is desirable to miniaturize capacitor required for an integrated circuit. $BaTiO_3$ and $SrTiO_3$ based ferroelectric materials exhibit high dielectric constant, but these materials show the strong temperature dependence of their dielectric constant which is not desirable from the device points of view (Chou *et al.*, 2007; Zhao *et al.*, 2007). Many research papers on high dielectric constant materials are available in literature since the last fifteen years of $ACu_3Ti_4O_{12}$ (A = Ca, $Bi_{2/3}$, $Y_{2/3}$, $La_{2/3}$, $Gd_{2/3}$) type perovskite (Homes *et al.*, 2001; Liu *et al.*, 2005). The correlation between the crystal structure and intrinsic dielectric properties the ceramic has been a controversial issue for several years, especially for $CaCu_3Ti_4O_{12}$ (CCTO), the most studied member of $ACu_3Ti_4O_{12}$ family. It exhibits high dielectric constant ($\varepsilon \sim 10^4$-10^5) which is independent of frequency (10^2-10^6 Hz) and temperature (100-600 K). This property is quite significant for microelectronic applications (Liu *et al.*, 2007; Homes *et al.*, 2001). However, at the same time, it exhibits high dielectric loss which limits its practical applications. Various explanations have been reported to explain the origin of a high dielectric constant phenomenon in $CaCu_3Ti_4O_{12}$ ceramic. The Internal barrier layer capacitor (IBLC) mechanism is widely accepted (Capsoni *et al.*, 2004), which assumes the existence of semi conducting grains and insulating grain boundaries. Different factors such as doping schemes (Chung *et al.*, 2006; Kwon *et al.*, 2008; Kobayashi *et al.*, 2003) as well as stoichiometric variations (Fang *et al.*, 2006; Shao *et al.*, 2007) influence the dielectric properties of CCTO. It is important to note that various isostructural materials based on complex perovskite structure, like $ACu_3Ti_4O_{12}$ (A = $Bi_{2/3}$, $Y_{2/3}$, $La_{2/3}$, $Nd_{2/3}$, $Sm_{2/3}$, $Gd_{2/3}$, $Dy_{2/3}$) also

exhibit similar dielectric properties with good thermal stability possessing (Liu *et al.*, 2005). All the three sites in $ACu_3Ti_4O_{12}$, viz, A, Cu or Ti-site, may equally facilitate the doping or partial substitution. The choice of substituent to modify the physical properties of the material is based on many factors including tolerance factor, ionic radius, charge neutrality and solubility. The partial isovalent substitution of metal cations in different interstices can improve properties associated with ferroelectricity and dielectric response in these materials due to the partial modification of mixed-valent structure. Further, structural flexibility and chemical versatility of the materials could make them more suitable for device applications and it is quite inspiring to investigate systematically new $ACu_3Ti_4O_{12}$ like materials.

A detail literature survey shows that only a limited number of research articles are available on $Y_{2/3}Cu_3Ti_4O_{12}$ (YCTO) compound which is isostructural to CCTO. Being non-ferroelectric, lead-free and eco-friendly too, YCTO material exhibits a high dielectric constant with good thermal stability. Liang *et al.* (2012) has prepared YCTO ceramic solid-state reaction method and reported the dielectric loss (tan δ) in kHz range only. Li *et al.* (2015) has discussed the phase formation with enhanced dielectric response of YCTO ceramics derived from Sol–Gel process. To our best knowledge, no work on the effects of doping in YCTO has been reported. In the present chapter, the partial doping in YCTO ceramic by Zn at Cu site has been described. An attempt has made to control the dielectric loss factor by such doping. The dielectric properties of $Y_{2/3}Cu_{3-x}Zn_xTi_4O_{12}$ (x = 0.10, 0.20 and 0.30) ceramic, simply abbreviated as YCZTO has been discussed. The microstructure of different samples of YCZTO has been investigated by XRD, SEM, EDX, AFM and TEM analysis.

5.2 RESULTS AND DISCUSSION

5.2.1 Thermal Analysis

The thermal analysis of dry precursor powder of YCZTO ceramic was carried out to know the ideal temperature required for thermal decomposition. Fig. 5.1 shows simultaneous TG/DTA/DTG plots of dry precursor powder of $Y_{2/3}Cu_{3-x}Zn_xTi_4O_{12}$ ceramic where (x = 0.10) at a constant rate of heating of 10 $^{\circ}C\ min^{-1}$ from ambient to 1000 $^{\circ}C$. The TG curve is characterized by two major stages of weight loss in the

temperature range from 100 °C to 1000 °C. The first at 250 °C may be due to an exothermic reaction which may be attributed to dehydration and combustion of the gel while the second weight loss at 830 °C may be attributable to the formation of an intermediate compound. Further, an additional but a slight weight loss at 950 °C was also observed which is due to an exothermic addition reaction of the intermediate compound to give the final product $Y_{2/3}Cu_{2.90}Zn_{0.10}Ti_4O_{12}$. The corresponding DTA and DTG plots also show two strong exothermic peaks near 250 °C and 850 °C besides a small peak at 950 °C. It is quite interesting that DTG peaks are more intense than DTA peaks.

5.2.2 X-Ray Diffraction Analysis

X-ray diffraction pattern of $Y_{2/3}Cu_{3-x}Zn_xTi_4O_{12}$ where (x = 0.00, 0.10, 0.20 and 0.30) ceramic sintered at 950 °C for 12 h is illustrated in Fig. 5.2. It clearly showed all the normal peaks of CCTO phase along with the presence of minor secondary phase of CuO (JCPDS 80-1917). The main XRD diffraction peaks of different YCZTO ceramic corresponding to (211), (220), (310), (222), (321), (400), (422), (440) planes were found to have a good matching with $CaCu_3Ti_4O_{12}$ (JCPDS card no. 75-2188). The sample with zinc concentration, x = 0.30 doesn't show single phase formation in the same sintering condition. We can extract an information that YCZTO ceramic exhibit sinle phase formation only upto, x = 0.20.

XRD data were indexed on the basis of a cubic unit cell similar to CCTO. The lattice parameter and unit cell volume of different YCZTO ceramic were calculated by least squares refinement method with the help of 'Cel' software and are shown in Table 5.1.The presence of split peaks in XRD pattern for the reflections 400, 422 and 440 may be due to the presence of Cu-Kα2 along with Cu-Kα1 in the X-ray radiations used for diffraction. From the line broadening of the main peaks, the crystallite size of the ceramic was estimated using the Debye Scherer formula (Culity *et al.*, 2001)

$$D = \frac{k\lambda}{\beta \cos\theta} \tag{5.1}$$

where k is the crystal shape coefficient (k = 0.89), λ is the wave length; β is the full width at half maximum (FWHM) and θ is the diffraction angle.

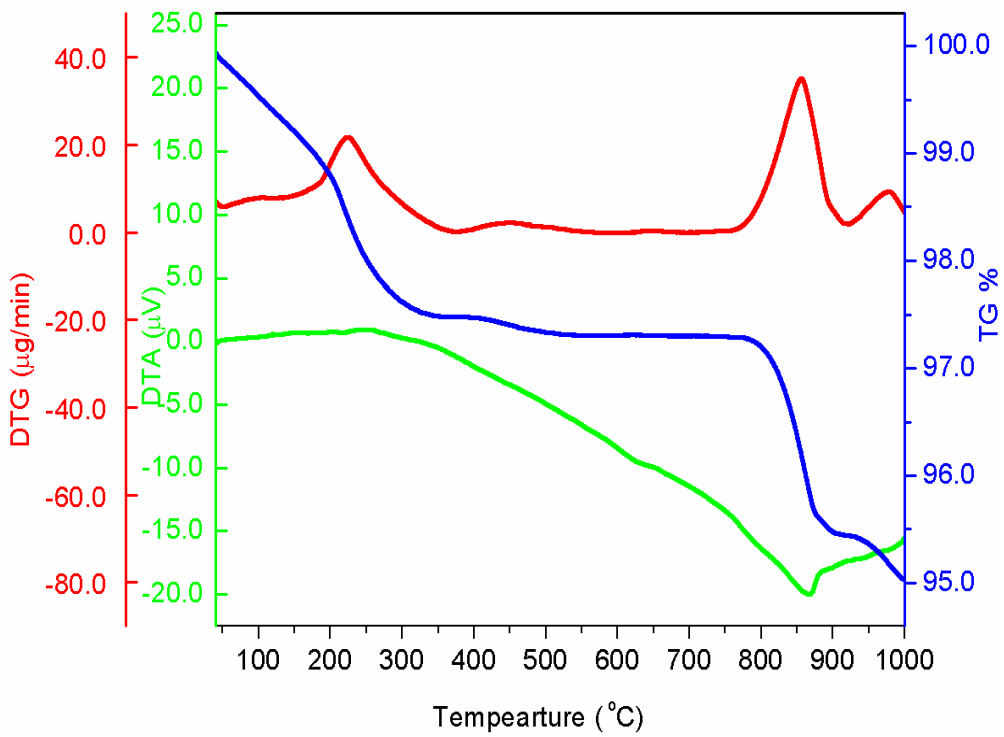

Figure 5.1: Plots of TG/DTA/DTG curve for the precursor powder of $Y_{2/3}Cu_{3-x}Zn_xTi_4O_{12}$ (x = 0.10) ceramic.

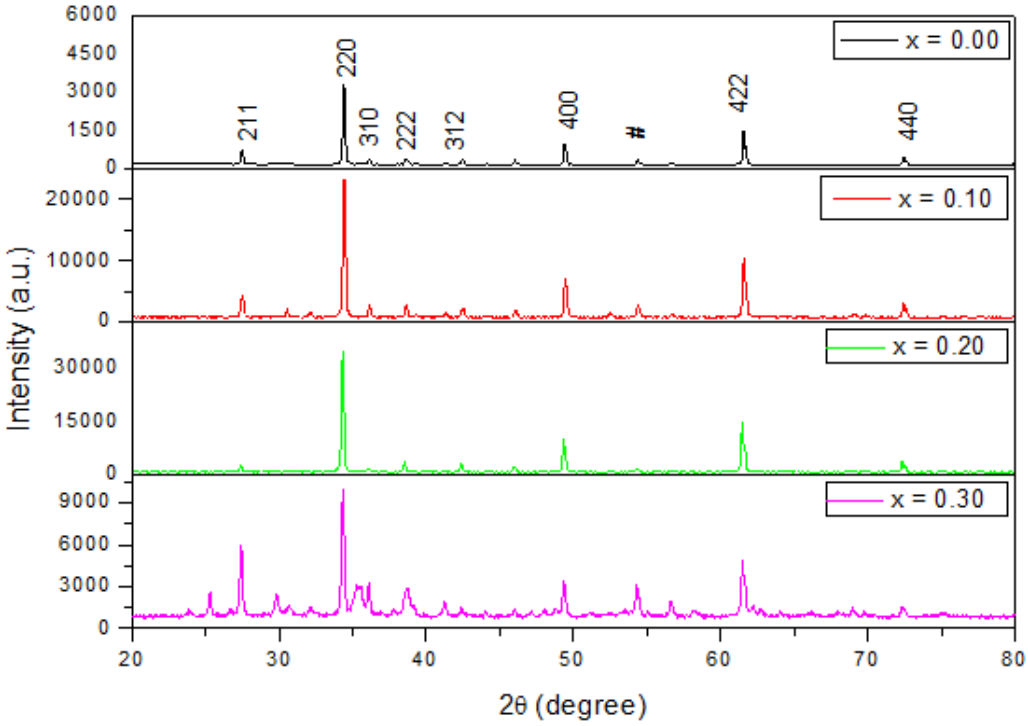

Figure 5.2: X-ray diffraction patterns of $Y_{2/3}Cu_{3-x}Zn_xTi_4O_{12}$ ceramic where (x = 0.10, 0.20 and 0.30) sintered at 950 °C for 12h.

After correction of instrumental broadening in the above equation, the estimated value of crystallite size for different YCZTO ceramic samples are shown in Table 5.1. It is observed from the table that the lattice parameter increases with an increase in the doping concentration of zinc ion. The change in unit cell parameter with doping concentration is due to increase in density.

Table 5.1: Lattice parameter, unit cell volume and particle size obtained from XRD for $Y_{2/3}Cu_{3-x}Zn_xTi_4O_{12}$ where (x = 0.00, 0.10, 0.20 and 0.30) ceramic

System	Composition	Structure	Lattice Parameter (Å)	Unit Cell Volume $(Å)^3$	Crystallite Size (nm) by XRD	Particle size (nm) by TEM
$Y_{2/3}Cu_{3-x}Zn_x Ti_4O_{12}$	x = 0.00	Cubic	7.4983	421.5833	68 ± 6	60 ± 20
	x = 0.10	Cubic	7.5035	422.2612	50 ± 10	39± 6
	x = 0.20	Cubic	7.5174	424.8154	56 ± 9	33 ± 5
	x = 0.30	Cubic	7.5211	425.4520	62 ± 9	_

5.2.3 Scanning Electron Microscopic and Energy Dispersive X-ray Spectroscopic Studies

Fig. 5.3 shows the scanning electron micrograph (SEM) of the fractured surface of undoped and zinc doped YCTO ceramic sintered at 950 $^{\circ}$C for 12h. The SEM micrograph exhibits smooth surfaced grains having bimodal structure with some pore like structures in samples, x = 0.00 and 0.10, however, sample with x = 0.20 contains very less pores. The microstructure is dominated by small spherical, cylindrical and some cubical grains. Some small grains of YCZTO sample with x = 0.00 are in the range of 1-2 µm, however, few irregular shaped large grains of size 2-3 µm are also observed without any secondary phases. The sample with x = 0.10 and 0.20 have grains size in the range of 0.5-1.5 µm. It is also noticeable that no distinct grain boundaries are present in these samples. The absence of grain boundary may be due to lower sintering temperature. The secondary phases were not observed in in

SEM micrographs. Such structures are analogous to the results obtained for CCTO sintered at low temperatures (Shao *et al.*, 2006; Pan *et al.*, 2005).

The composition of grains coincides with the stoichiometric of YCZTO which is also supported by EDX results. The variation in grain size thereby leading to abnormal grain growth may be due to the presence of CuO rich phase in their samples of YCZTO. Fang *et al* (2007) also reported the presence of CuO along the grain boundary which transforms into the liquid phase during sintering it may instigate a discontinuous grain growth which is in accordance with the SEM micrograph of Fig. 5.3. The CuO phase may contribute significant effects to promote the grain growth and densification of YCZTO ceramic. It is also established that increase in sintering temperature significantly promote the grain growth and microstructural densification. Further, it is reported in literature that below 1µm, the dielectric constant decreases significantly with grain size. As the grain size approaches to 0.5- 1.5 µm, the various types of stress operating in the grain suppress the domain and the dielectric constant falls to approximately 1000 (Moulson *et al.*, 2003). However, there seems no such relation between the grain size and dielectric constant value for YCZTO ceramic. Besides grain size in the range of 0.5-1.5 µm, YCZTO exhibits high dielectric constant value (ε ~18552) than the pure YCTO ceramic (ε ~8434) with grain size in the range of 1-3µm which may be due to porosity, compactness of grain and the structural quality of the material. It is also clear from the Fig. 5.3 that YCZTO ceramic shows high degree of porosity. Correspondingly, the porosity of the ceramic was measured with the help of Archimedes principle and was calculated through the following formula:

$$\rho = \frac{W_1 - W_2}{W_1 - W_{3.}} \times 100\% \qquad (5.2)$$

Here W's corresponds to the wet weight (W_1), dry weight (W_2) and buoyant weight (W_3) while 'ρ' describes the porosity of YCZTO ceramic. The calculated value of apparent porosity in YCZTO (x = 0.00, 0.10 and 0.20) ceramic was found to be 5.6, 9.05 and 10.5 %. The high porosity may be attributed to the formation of oxygen vacancies during sintering. It may be also due to lower sintering temperature. Increase in sintering temperature may lead to decrease in porosity owing to the grain growth phenomena. Moreover, the porosity also depends upon processing route.

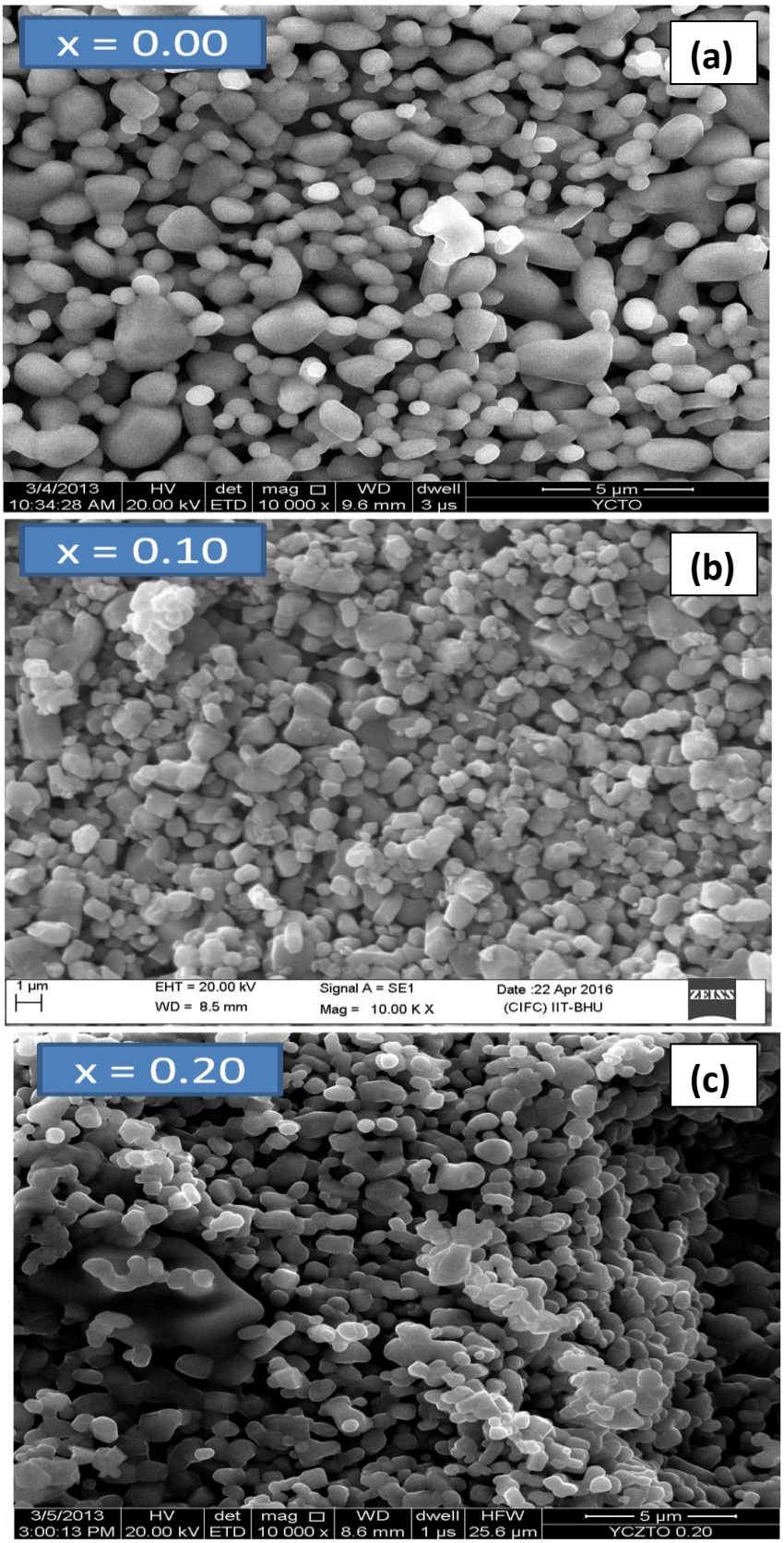

Figure 5.3: SEM micrographs of $Y_{2/3}Cu_{3-x}Zn_xTi_4O_{12}$ (a) x = 0.00 (b) x = 0.10 (c) x = 0.20 ceramic sintered at 950 $^{\circ}$C for 12h.

Samples prepared by Pechini method and co-precipitation method exhibit a lower extent of porosity than those prepared by other processes at the same sintering temperature (Niwa *et al.*, 2012). It was also observed that doping of Zn in YCTO ceramic causes decrease in density and increase in porosity. The theoretical density of different YCZTO ceramic was found to be 5.995, 5.989, 5.947 and 5.955 g/cm^3 respectively for the compositions x = 0.00, 0.10, 0.20 and 0.30. It is in accordance with the reported value of undoped YCTO ceramic (Liang *et al.*, 2012).

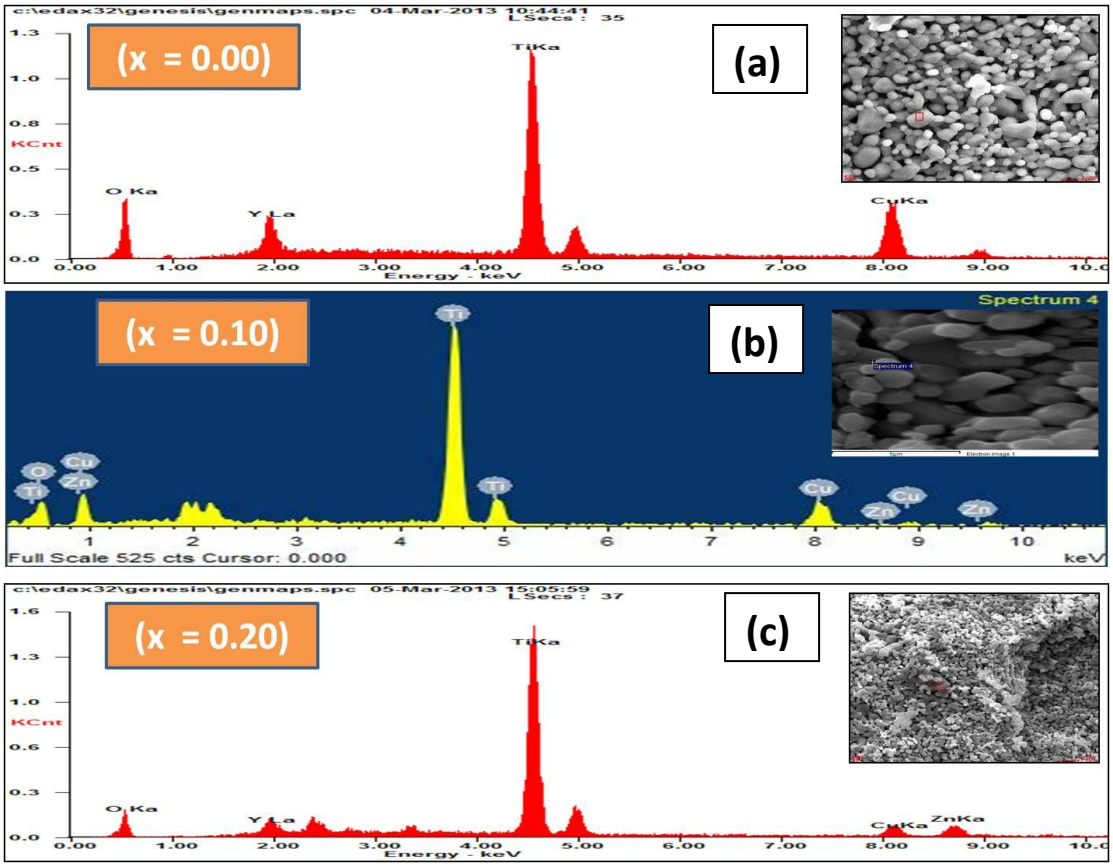

Figure 5.4: EDX spectra of $Y_{2/3}Cu_{3-x}Zn_xTi_4O_{12}$ (x = 0.00, 0.10, and 0.20) sintered at 950 $^{\circ}$C for 12h

Fig. 5.4 shows EDX spectra of a grain of different compositions of $Y_{2/3}Cu_{3-x}Zn_xTi_4O_{12}$ (x = 0.00, 0.10, and 0.20) which confirms the presence of Y, Cu, Zn Ti and O elements. The atomic percentage of Y, Cu, Zn Ti and O elements in

different compositions of $Y_{2/3}Cu_{3-x}Zn_xTi_4O_{12}$ ceramics were found as per expected stoichiometry of the YCZTO ceramic which confirms the purity of theses samples.

5.2.4 Atomic Force Microscopic (AFM) Studies

The surface topography of $Y_{2/3}Cu_{3-x}Zn_xTi_4O_{12}$ ceramic with composition x = 0.10 was studied with the help of Atomic force microscopy. These images were obtained by a thin film deposition on the glass substrate in a tapping mode. AFM study discloses the average roughness (R_a), skewness (R_{sk}), and kurtosis (R_{ku}). The surface roughness estimated from AFM image is usually the "local" roughness. The average roughness is an arithmetic average of the height of the surface asperities, above a hypothetical, smooth plane. The skewness shows the degree of symmetry of the rough surface profile and can be used as a measure of the balance between the peaks and valleys of the asperities while the kurtosis shows the degree of sharpness or bluntness of the asperities on the surface. Fig. 5.5(a) represents the 2D AFM images of YCZTO which is characterized by the bright and dark contrast in the grains shows topological variations, with the brighter regions being higher. Fig. 5.5(b) shows two-dimensional AFM image of the grains and grain boundary of YCZTO ceramic. It exhibits compact structure with granular morphology, buffer layer, plates like grains and clear grain boundary. Fig. 5.5(c) exhibits its 3D surface morphology exhibits several peaks corresponding to grain with compact structure. The maximum peak height of the grain is 3.668μm within the scanning area 20μm × 20μm. The average grain size and average diameter of grain was estimated to be 90.8 nm (Fig. 5.6a) and 102.4 nm (Fig. 5.6b), out of 301 grains as exhibited by 3D-AFM histogram, when the grains were homogeneously mounted over the substrate of an area 0.0943 μm^2 (Fig. 5.6c). Fig. 5.6(d) shows the corresponding surface roughness. Through the roughness parameters, the surface condition of the entire measured length or area will be evaluated in terms of peak and valley (Raposos et al 2007).

Based upon the statistical study of total 65536 grain ensembles, the value of average surface roughness and root mean square roughness was found to be 0.346 and 0.424 μm within the scanning area 20μm × 20μm. The skewness was found to be 0.0107 which is nearly equal to zero and kurtosis to be 3.224, a value exceeding 3. Apart from the average roughness, the lower positive values of skewness roughness (R_{sk}) imply for the smoothness of surface with predominant peaks while higher positive value for kurtosis roughness (R_{ku}) indicating that the surface of scanned area

of YCZTO thin film is slightly bumpy in nature due to the appearance of low number of high peaks and low valleys on the surface. As kurtosis value is more than three, such distribution curve has many high peaks and low valleys. It is more evident from the 3D image (Fig. 5.5 C). Thus, AFM analysis provides a wider range of particles distribution in the YCZTO ceramic.

The surface roughness parameters of the tested sample in 2D and 3D AFM study of YLCTO thin film, deduced with the help of NOVA software are summarized in Table 5.2.

Table 5.2: The surface roughness parameters of $Y_{2/3}Cu_{3-x}Zn_xTi_4O_{12}$ (x = 0.10) thin film obtained by 2D- and 3D- AFM-image mapping.

Details of Roughness	**Parameters**	
	Amplitude (2D)	**Height (3D)**
Average /Arithmetic	0.261	0.366
Root Mean Square	0.359	0.424
Maximum peak to valley height roughness	1.943	3.672
Ten-points mean height roughness	1.020	3.047
Skewness	0.0473	0.0107
Kurtosis	3.568	3.224

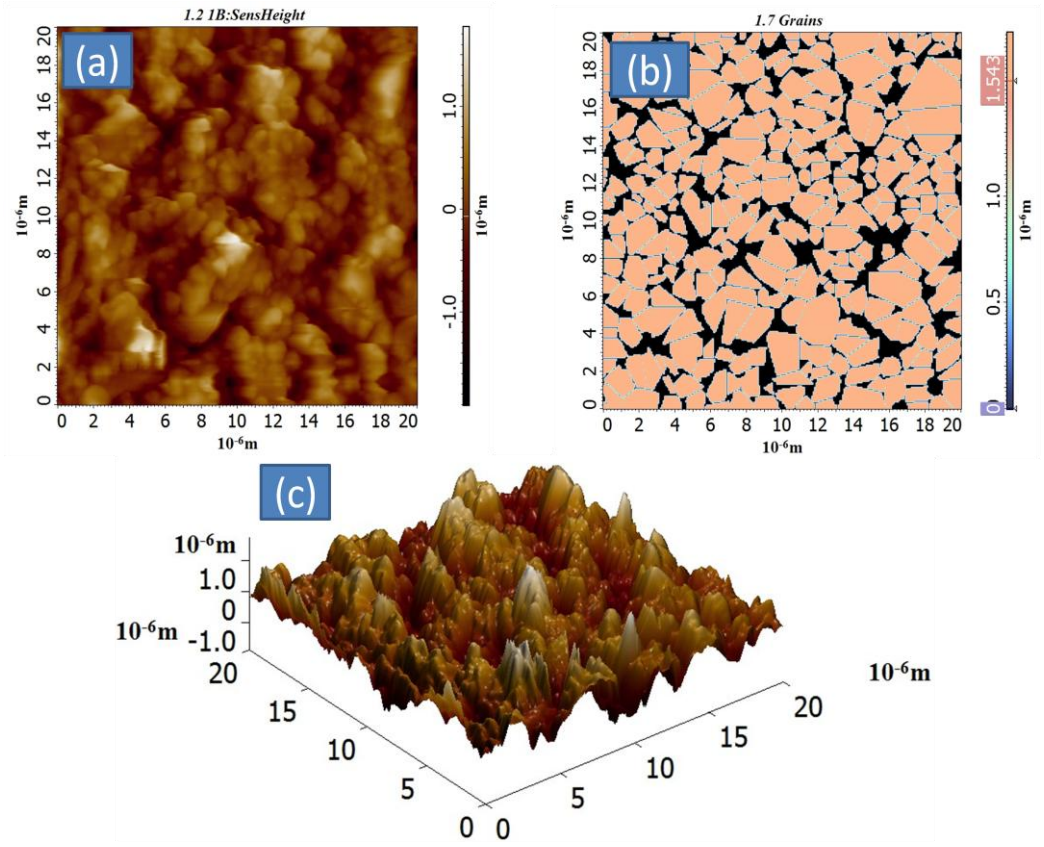

Figure 5.5: (a) 2- dimensional AFM micrograph of thin film of (b) 2-dimensional AFM micrograph showing grain boundary (c) 3- dimensional AFM micrograph of sintered $Y_{2/3}Cu_{3-x}Zn_xTi_4O_{12}$ (x = 0.10) ceramic.

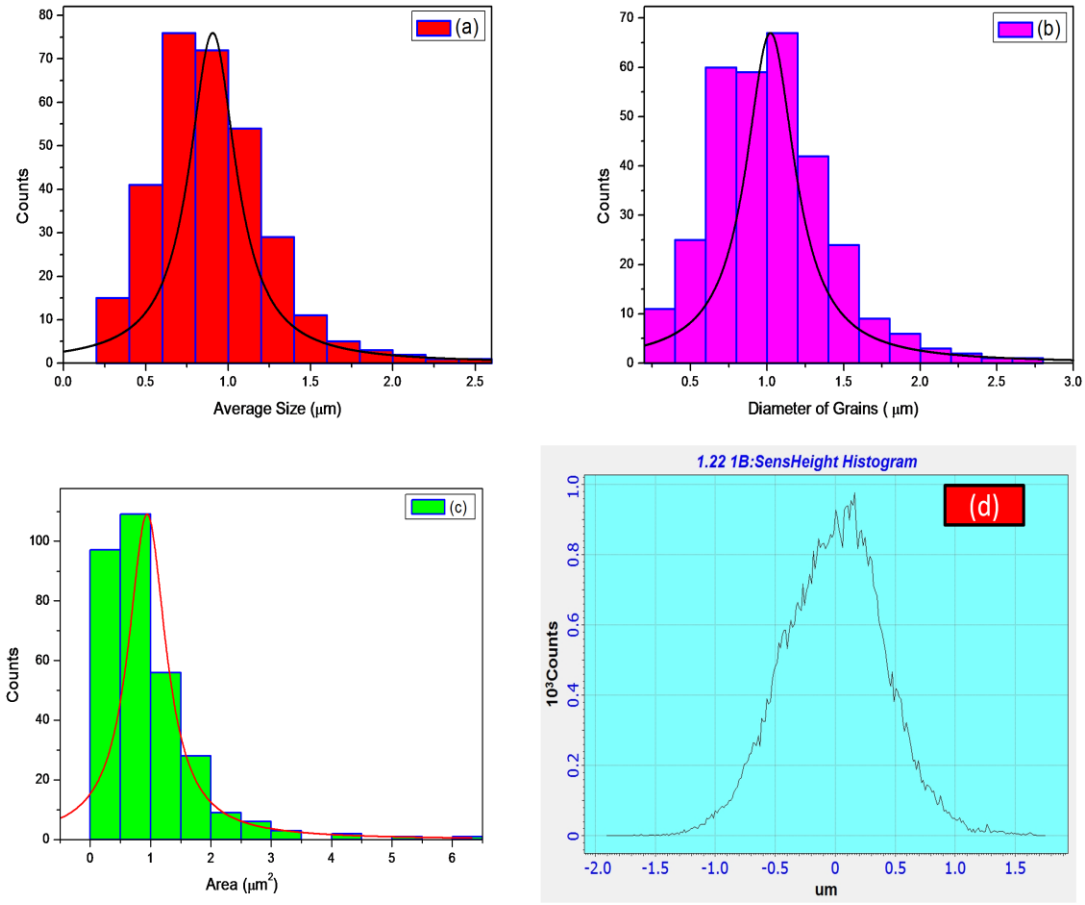

Figure 5.6: Different histograms for sintered $Y_{2/3}Cu_{3-x}Zn_xTi_4O_{12}$ (x = 0.10) ceramic exhibiting (a) Average size (b) Diameter of grains (c) Area of grains and (d) Average 3 - dimensional roughness.

5.2.5 Transmission Electron Microscopy

`The bright field TEM image along with the corresponding selected area electron diffraction (SAED) pattern of different sintered $Y_{2/3}Cu_{3-x}Zn_xTi_4O_{12}$ ceramic with x = 0.00, 0.10 and 0.20 is shown in Fig. 5.7. SAED patterns are a projection of the reciprocal lattice, with lattice reflections showing as sharp diffraction spots. By tilting a crystalline sample to low-index zone axes, SAED patterns can be used to identify crystal structures and measure lattice parameters. It is essential for setting up dark-field imaging conditions. It is important to note that SAED of polycrystalline materials gives ring patterns analogous to those from X-ray powder diffraction. However, the presence of a few clear rings in SAED pattern [Fig. 5.7 (b) and (d)] confirms the formation of polycrystalline phase of thermodynamically stable YCZTO ceramic. It also supports the XRD findings. However, a few single spots may appear only, as seen in Fig 5.7 (e), when the beam gets diffracted by a single crystal. In some cases there may exist many crystals with different orientations with the same material (Carter et al., 2009). The particles of are well dispersed with high extent of agglomeration. The average particles size of different YCZTO samples is also shown in the Table 5.1. However, the particle size obtained by TEM analysis is lesser than XRD results because a crystallite may consist of several particles. It is important to note that with the help of TEM particle size is measured but with XRD we measure the crystallite size which is the coherent diffracting crystalline domains (crystallite), which is different from the particle size. One particle can be constituted by several crystalline domains (crystallites), this is why always particle size has to be bigger than crystallite (domain) size, or in case of small nano particles both of them can be the same. But the domain size or crystallite size, calculated from XRD, cannot be bigger than particle size obtained from TEM (Carter et al., 2009).

TEM diffraction patterns (SAED) were indexed on the basis of body centered cubic perovskite structure. The lattice parameter calculated from the electron diffraction pattern is also supports the findings from the XRD result. The zone axis of the selected area electron diffraction (SAED) of the YCZTO ceramic was calculated which was found to be $[\bar{1}, 3, \bar{1}]$.

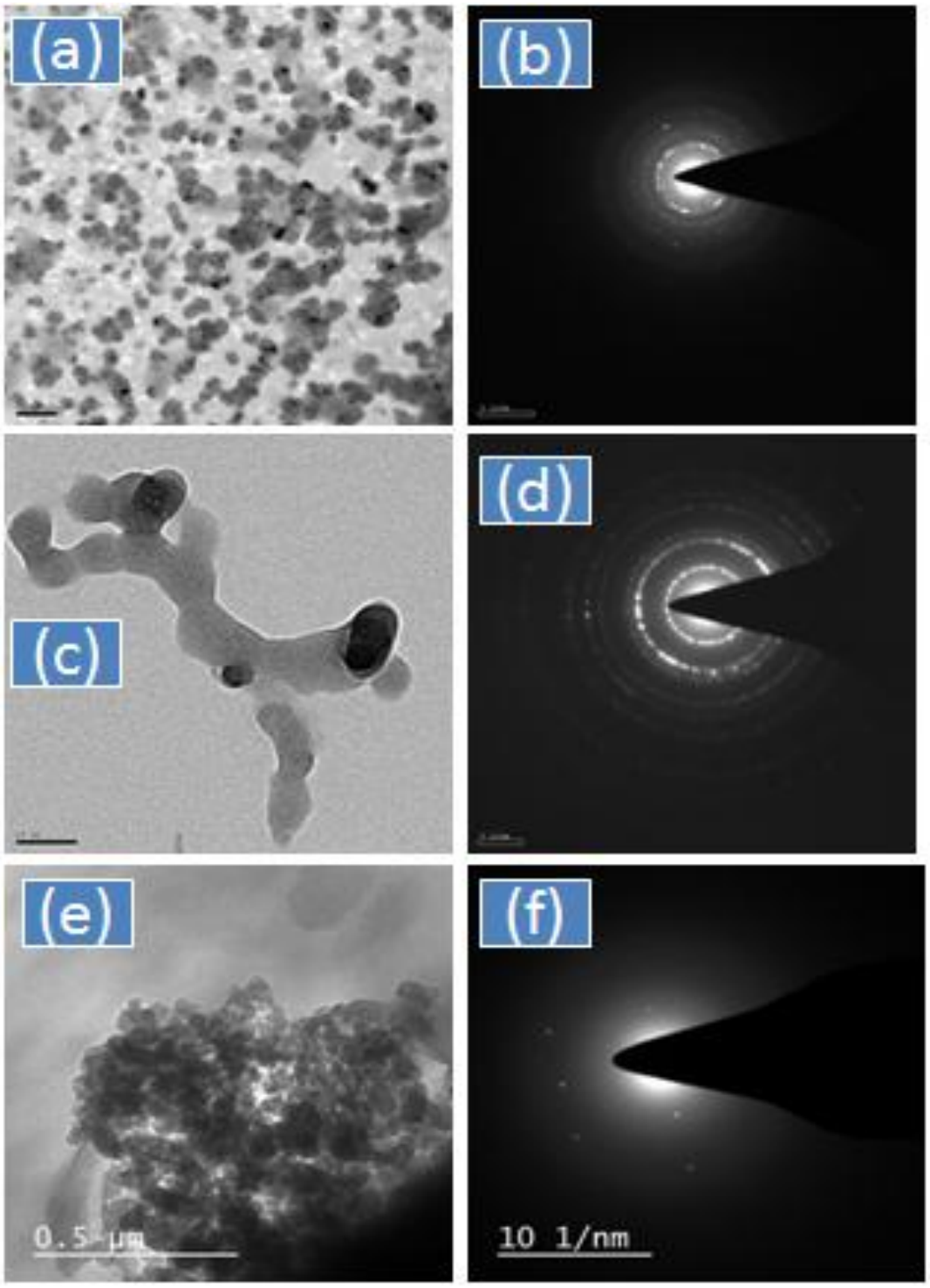

Figure 5.7: Bright Field TEM images of $Y_{2/3}Cu_{3-x}Zn_xTi_4O_{12}$ ceramic sintered at 950 °C for 12h. (a) x = 0.00 (c) x = 0.10 and (e) x = 0.20 and (d) their corresponding SAED patterns (b) x = 0.00 (d) x = 0.10 (f) x = 0.20.

5.2.6 P-E Loop measurement

The origin of polarization and ferroelectric behavior of ceramic may be justified with the help of polarization electric (P-E) Loop tracer technique. PE hysteresis loop is related to its energy storage ability and it displays significant material property of dielectric materials. This loop can be discussed in terms of three important parameters viz. remnant polarization (P_r), saturated polarization (P_s) and coercive field (E_c) under the external electric field. The PE hysteresis loop obtained at 308 K for $Y_{2/3}Cu_{3-x}Zn_xTi_4O_{12}$ (x = 0.10) ceramic is shown in Fig. 5.8. The value of remnant polarization (Pr), saturation polarization and coercivity (E_C) are found to be 0.206 μCcm^{-2}, 0.971 μCcm^{-2} and 0.477 $kVcm^{-1}$, respectively. This may be due to the alignment of domains present in the ceramic which increases with temperature in absence of electric field. Another reason may be the display of high dielectric constant phenomenon, contributing significantly to the relaxor-ferroelectric behavior (Raya *et al.*, 2013).

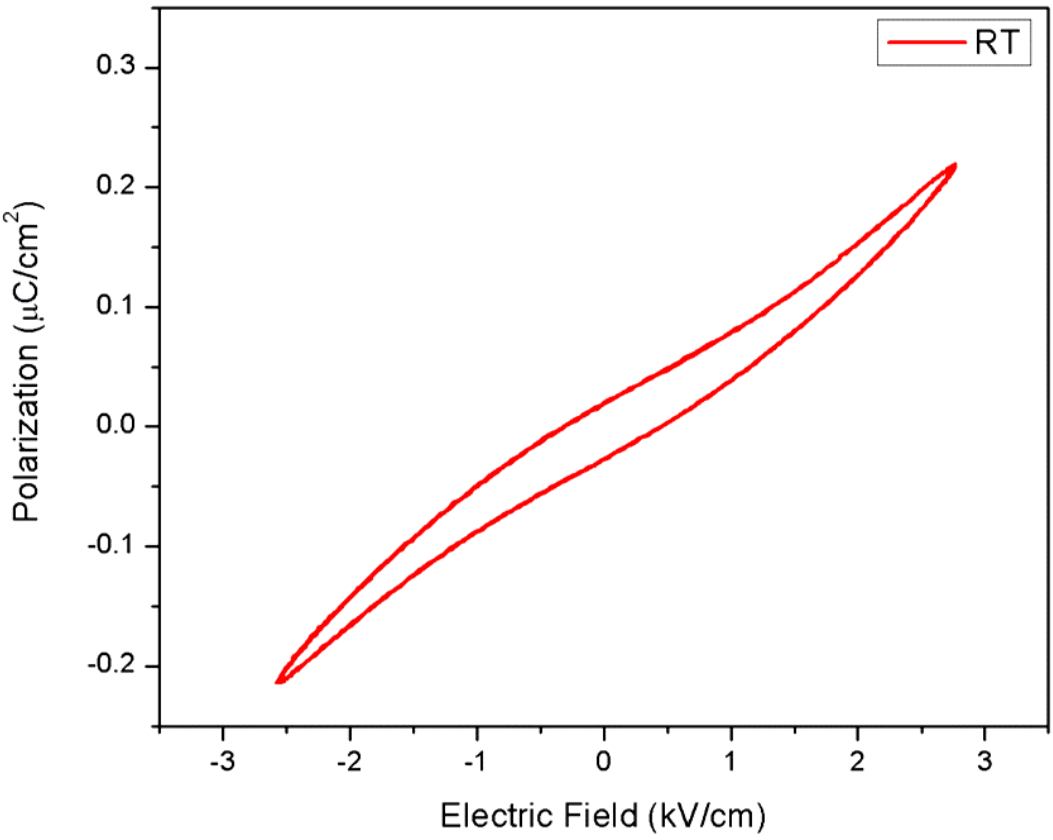

Figure 5.8: Polarization hysteresis loop of sintered $Y_{2/3}Cu_{3-x}Zn_xTi_4O_{12}$ ceramic (x = 0.10).

5.2.7 Dielectric and Electric Behavior

The effect of temperature variation on dielectric constant (ε) and dielectric loss (tan δ) of YCZTO ceramic has been studied in detail. The dielectric measurement were carried out in the temperature range of 308-500 K at an interval of 20 K. Fig. 5.9 exhibits the variation of dielectric constant (ε) and dielectric loss (tan δ) as a function of temperature for different YCZTO ceramics at a few selected frequencies (0.1, 1, 10, 100 kHz). For all synthsesize samples exhibits a slight increase in dielectric constant with temperature in low frequency range, however, the increase in temperature shows a remarkable change at high frequency. It is clearly observed from the plot that the dielectric constant in higher frequency range (10 kHz and 100 kHz) is almost temperature independent under the investigated temperature range, however, in case of sample with composition x = 0.20 and 0.30 (Fig. 5.9 II), the dielectric constant increases smoothly above 425K. In fact the dielectric constant exhibits a step increase with increasing temperature after the dispersion peak. Such type of dielectric behaviour is similar to those of CCTO reported earlier (Rai *et al.*, 2009).

Sample with composition x = 0.00 i.e. undoped YCTO ceramic, as discussed in section 3.2.6 (Chapter 3), exhibits a broad dielectric dispersion peak from 350-450 K. Below this temperature dielectric constant increase from a low value 8434 at room temperature (308 K) to a high value 12849 at 353K and then decreases to 1072 at 425 K. However, it exhibits almost frequency independent dielectric constant above 450 K.

The intensification of a broad dielectric peak which gets suppressed further at higher frequency is a clear indication of relaxor behavior in the ceramic. A relaxor behavior is usually characterized by diffuse phase transition and strong relaxational dispersion in dielectric constant and loss tangent (tan δ) which may be due to thermally activated relaxation (Cross 1994). However, the broadness as well as height of dispersion peak gets decreased in case of composition x = 0.10 and almost disappears in case of composition x = 0.10. The decrease in relaxor property or its complete absence in zinc dopes YCTO ceramic is really appreciable from application point of view.

The composition x = 0.30 also shows a sign of dispersion peak at room temperature (308 K). A clear peak may be obtained for this ceramic below the experimental temperature.

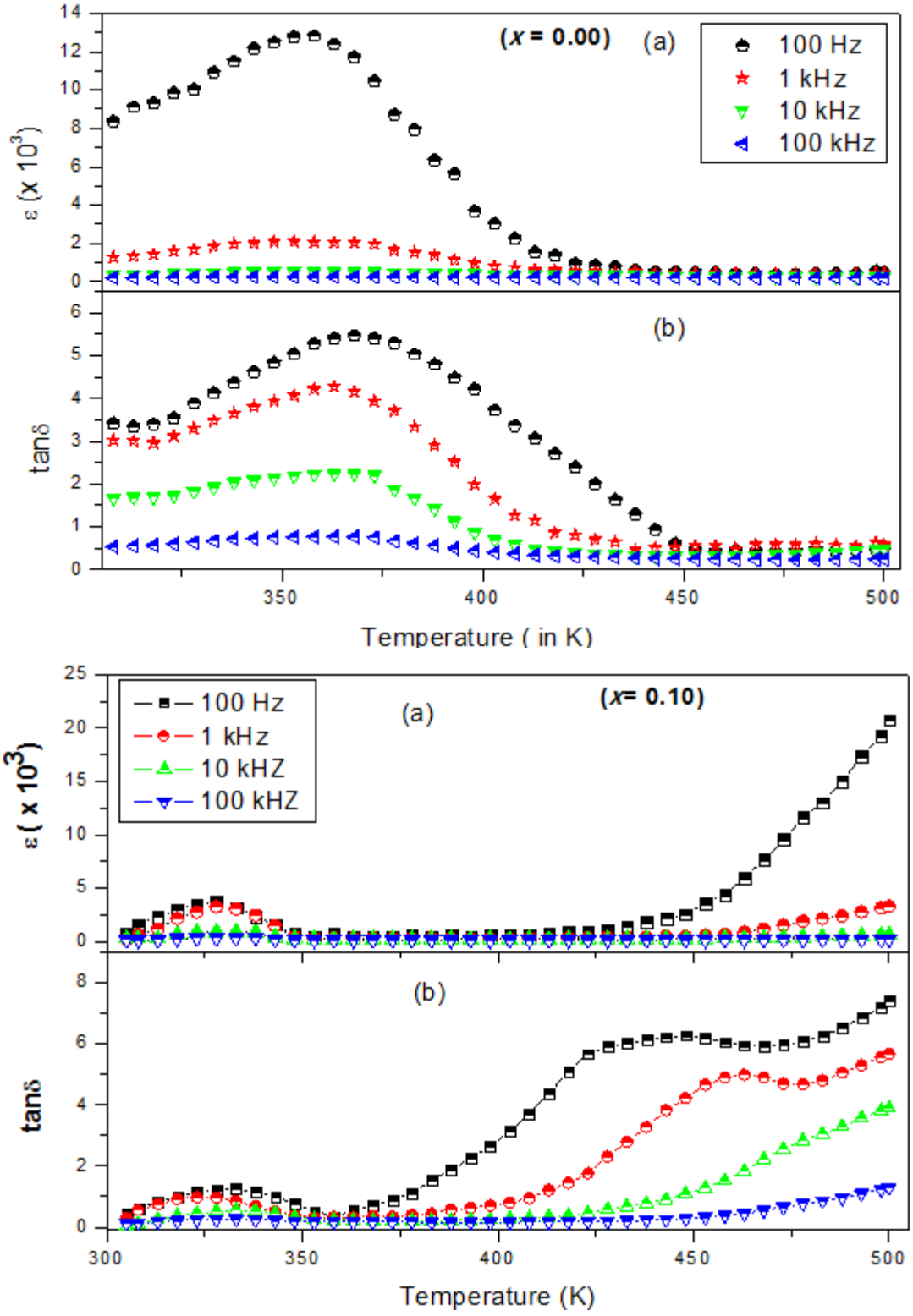

Figure 5.9(I): Variation of dielectric constant (ε′) and loss tangent (tan δ) with temperature at few selected frequencies for $Y_{2/3}Cu_{3-x}Zn_xTi_4O_{12}$ ceramic (x = 0.00 and 0.10) sintered at 950 °C for 12h.

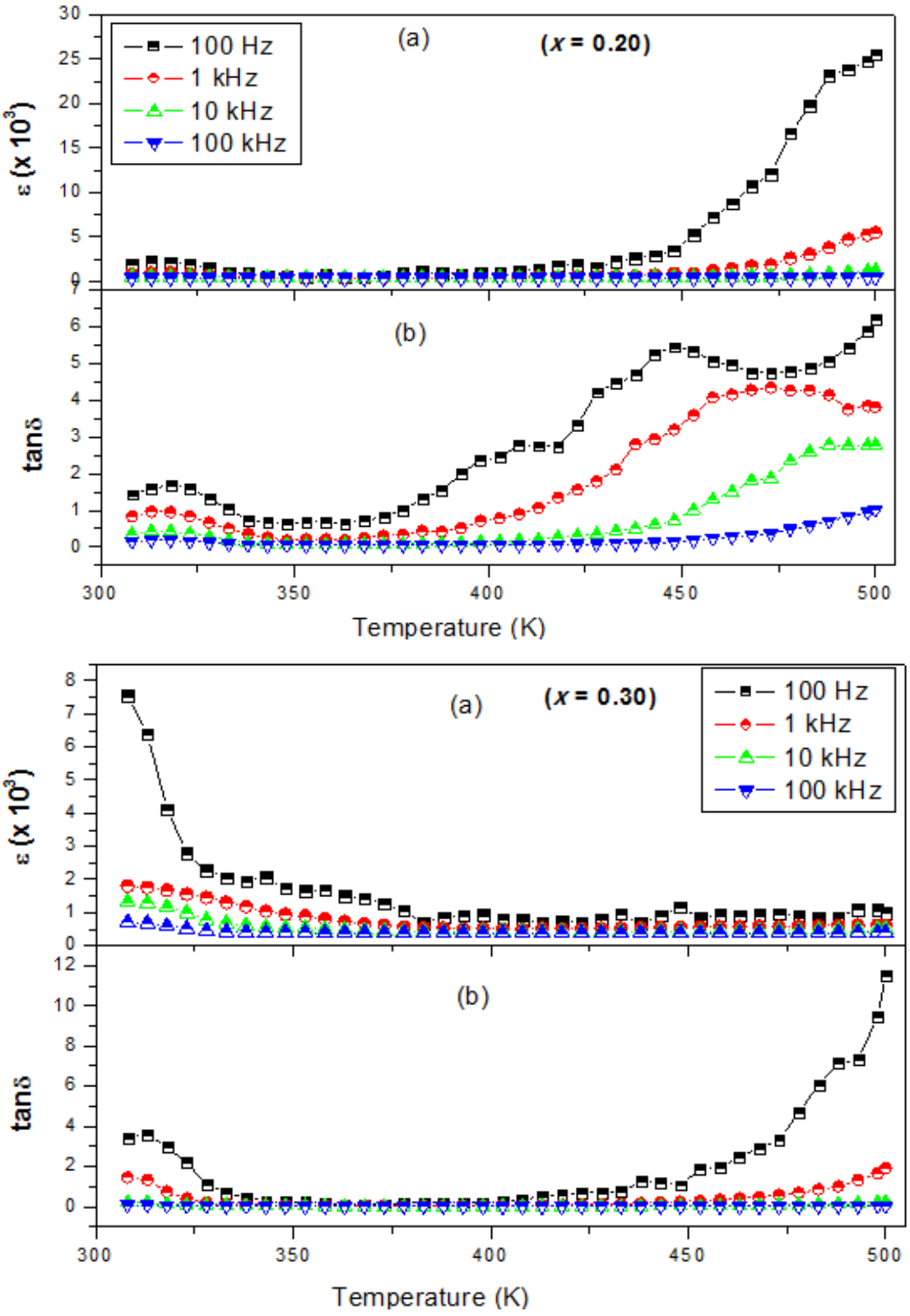

Figure 5.9 (II): Plots of dielectric constant (ε′) and loss tangent (tan δ) with temperature at few selected frequencies for $Y_{2/3}Cu_{3-x}Zn_xTi_4O_{12}$ ceramic (x = 0.20 and 0.30) sintered at 950 °C for 12h.

In case of zinc doped YCTO ceramic, the low frequency (100 Hz and 1 kHz), dielectric dispersion peaks was observed below 350 K for composition x = 0.10. But the value of dielectric constant increases sharply to a higher value above this temperature. At 100 Hz, the value of dielectric constant increases from 886 at 303 K to 3775 at 327 K and then decreases to 826 at 347 K. However YCZTO ceramic shows exceptionally very high dielectric constant value (ε ~20774 at 100 Hz and 500 K) compared to other frequencies. An increase in the value of dielectric constant with increase in temperature may be attributed to fact that as temperature increases, the orientation of interfacial polarisation get facilitated which enhances dielectric constant value. But at lower frequency the rapid increase in dielectric constant with temperature may be due to the polarisation due to interfacial diploes which are strongly temperature dependent, however, as temperature increases, the accumulation of charge at the grain boundary increases which induces an increases in dielectric polarization. Therefore, it is the dielectric polarization which causes increase in dielectric constant value with increases in temperature at lower frequencies. It is also observed from the Fig. 5.9 I and II (a) that the value of dielectric constant increases with temperature in contrast to CCTO which shows almost independent variation with temperature. An increase in dielectric constant value is always accompanied with loss tangent peaks which signify the presence of the high temperature dielectric relaxation in YCZTO ceramic.

The high temperature dielectric relaxation may arise from an extrinsic mechanism as well as the presence of defects or oxygen vacancies produced during sintering and cooling mechanisms while the low temperature relaxation in different YCZTO ceramic supports the grain boundary effect. The presence of broad dielectric peak obtained for 100 Hz and 1 kHz below 350 K, which gets suppressed at higher frequency, confirms the presence of ferroelectric relaxor behavior in the YCZTO (Parkash *et al.*, 2008).

The variation of dielectric loss (tan δ) as a function of temperature [Fig. 5.9 I and II (b)] which is characterized by the presence of same type of dispersion peaks below 350 K. YCZTO ceramic shows a diminished dispersion peaks with several humps which is due to relaxation behavior, however, such relaxation peaks gets intensified in case of YCZTO ceramic with composition x = 0.0. The dielectric losses for YCZTO ceramic at 350 K were found to be 0.47, 0.32, 0.10, and 0.02 at 0.1, 1, 10,

100 kHz, respectively. The presence of dispersion peaks in both the figures ε-T and tan δ-T below 350 K and at lower frequencies (i.e. less than 1 KHz) supported the presence of Maxwell-Wagner type of relaxation phenomena in the ceramic. The presence of low frequency relaxation may be attributed to the occurrence of space charge polarization arising at the interface of grain and grain boundary which has a large difference in their electrical conductivity. It is clearly seen that the value of tan δ increases with increases in temperature. A rapid increase in tan δ at higher temperatures may be due to exponential increase of conductivity with temperature as observed normally.

Fig. 5.10 illustrates the frequency dependence of ε′ of different sintered YCZTO ceramics at a few selected temperatures. It is clearly observed that dielectric constant decrease gradually with increase in frequency. This decrease is more prominent in the low frequency region which may be explained in terms of relaxation of dipoles at the grain boundary as well as due to the contribution of interfacial effects due to ceramic-electrode combination.

The value of ε′ YCZTO ceramic was found to be 18552, 149846, 600000 with composition x = 0.10, 0.20, 0.30 respectively at 308 K and 100 Hz while undoped YCTO ceramic exhibits the dielectric constant value equals to 8434 at the same temperature and frequency which is much higher than the undoped one. It is also clear that the value of dielectric constant (ε′) decreases steeply in lower frequency range whereas it decreases slowly in higher frequency range (1 kHz-5 MHz). The decrease in dielectric constant with frequency may be due to the contribution of space charge accumulation at the interface which leads to polarization of the ionic medium and hence increases the value of ε′. In high frequency regions, the periodic reversal of the field takes place so rapidly that there is no charge accumulation at the interface, resulting into a constant ε′ value (Tareev 1975).

Besides the value of ε′ and tan δ, the temperature coefficient (Δε′), is one of the most important parameter, which must be considered. The temperature coefficient (Δε′) is basically the temperature dependence of ε′ within a certain temperature range, which suggests the compatibility of any desired material for appropriate capacitor and resonator applications. The temperature coefficient (Δε′) for YCZTO ceramic was calculated at a frequency of 1 kHz and may be defined as

$$\Delta\varepsilon = \frac{\varepsilon'_T - \varepsilon'_{20}}{\varepsilon'_{20}} \times 100[\%] \qquad [5.3]$$

where ε'_T and ε'_{20} are the value of real part of dielectric constant (ε′) at a temperature T °C and 20 °C, respectively. The calculated value of Δε′ was lower than 15% in the temperature range 308-500 K, for compositions x = 0.10 and 0.20, indicating thereby the potential use of YCZTO ceramic as a capacitor device.

Dielectric absorption in a material is generally characterized by tan δ as well as dielectric loss (ε″) values. Usually a relaxation peak is obtained at a specific frequency and temperature when ε″ and tan δ values are plotted against frequency. Such type of dielectric relaxation occurs when hopping frequency of charge carriers is equal to the frequency of the applied field. However, such relaxation peaks were absent in case of YCZTO ceramic with compositions x = 0.10 and 0.20, when imaginary part of dielectric constant (ε″) is plotted against frequency as shown in Fig. 5.11.

Undoped YCTO and YCZTO ceramic composition x = 0.30 give the direct evidence for relaxor behavior quite well. Such type of dielectric relaxation in YCTO is encountered around 10^5-10^6 Hz frequency (Fig. 5.11 I). YCZTO ceramic with composition x = 0.30 also exhibits very interesting relaxation peaks around 10^3-10^7Hz frequency at all temperatures. These relaxation peaks gets suppressed and shifted to higher frequency region from temperature 428-508K. Such variation establishes the existence of Maxwell- Wagner relaxation in this composition. The absence of relaxation peaks in YCZTO ceramic with composition x = 0.10 and 0.20 may be attributed to reduction in the number of hopping charges available for hopping as the concentration of Zn increases. It is likely that the relaxation peaks corresponding to YCZTO ceramic may lie outside the measuring frequency range.

Fig. 5.12 shows the variation of loss tangent (tan δ) with frequency at a few selected temperature (308-500 K) which is characterized by the presence of relaxation peaks. These peaks shift to higher frequency regimes with increase in temperature which may be attributed to the presence of Maxwell Wagner relaxation. YCZTO ceramic shows high dielectric constant (ε ~7183) and low dielectric loss (tan δ ~0.76) at 368 K and 2 Hz. The dielectric loss of YCZTO ceramic was found to be 0.2 to 1.03 (308 to 428 K) and 2.3-3.38 (468- 500 K) at 1 kHz frequency.

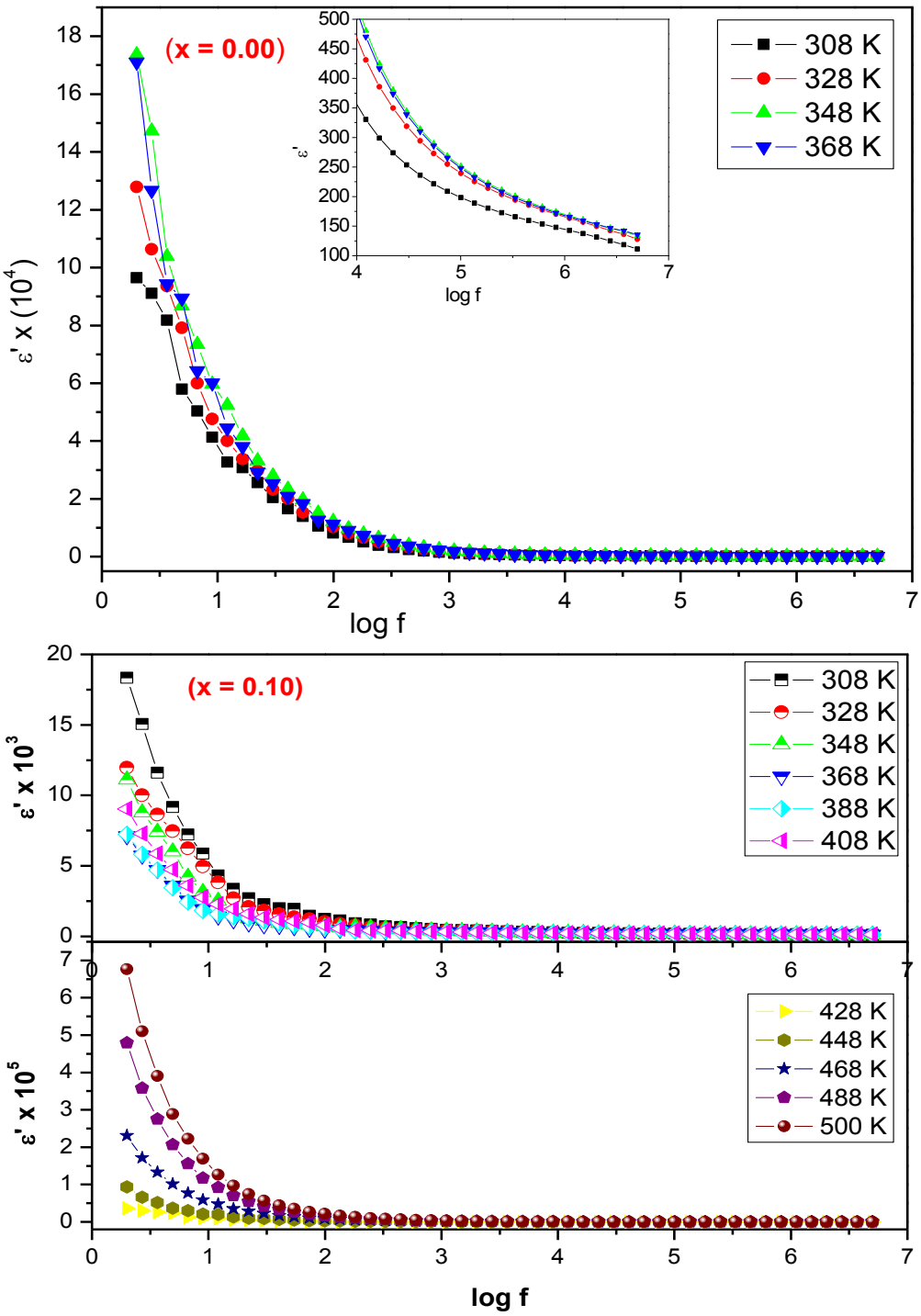

Figure 5.10 (I): Variation of the real part of dielectric constant (ε′) with frequency at few selected temperatures for $Y_{2/3}Cu_{3-x}Zn_xTi_4O_{12}$ ceramic (x = 0.00 and 0.10) sintered at 950 °C for 12h.

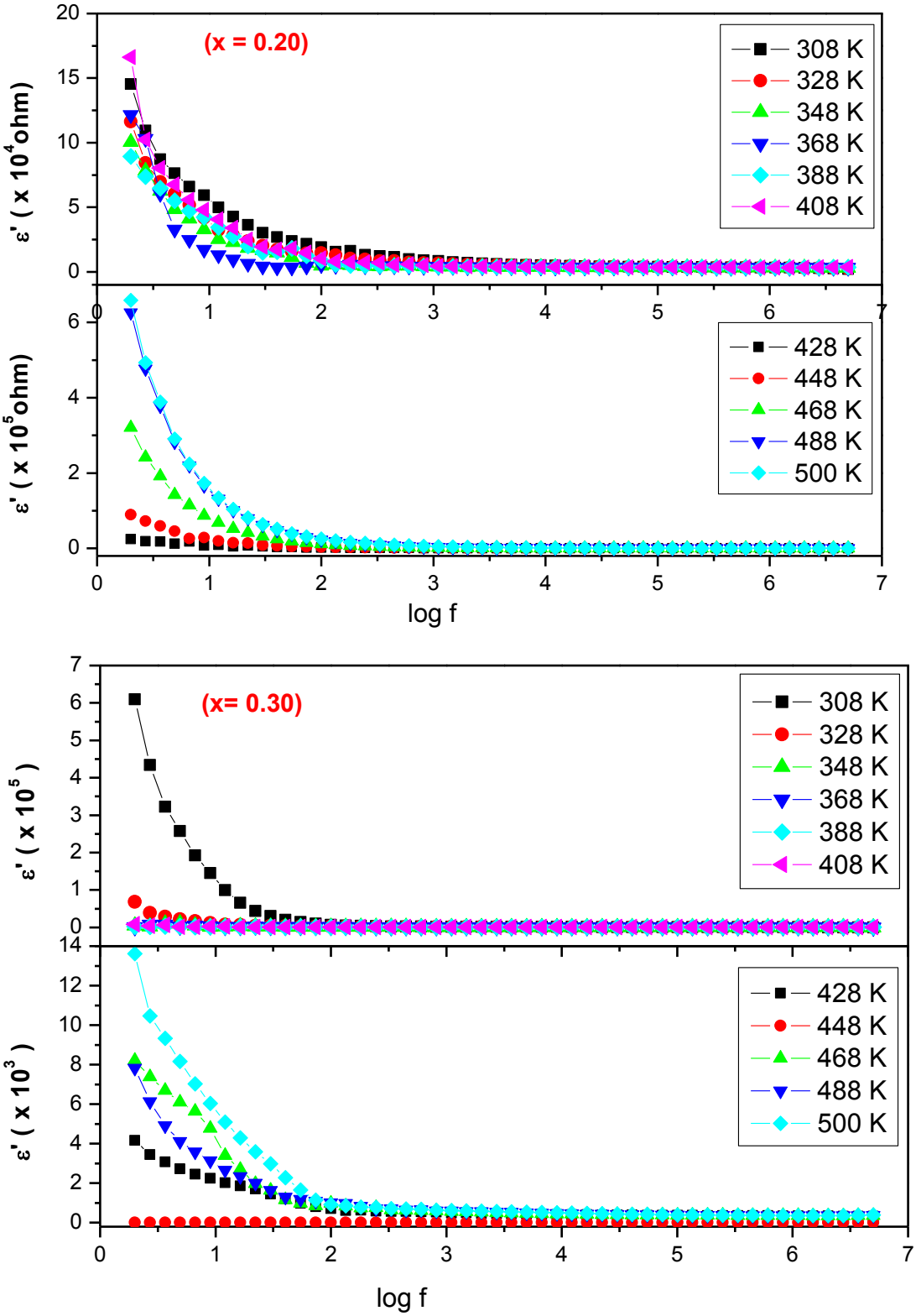

Figure 5.10 (II): Variation of the real part of dielectric constant (ε′) with frequency at few selected temperatures for $Y_{2/3}Cu_{3-x}Zn_xTi_4O_{12}$ ceramic (x = 0.20 and 0.30) sintered at 950 °C for 12h.

.

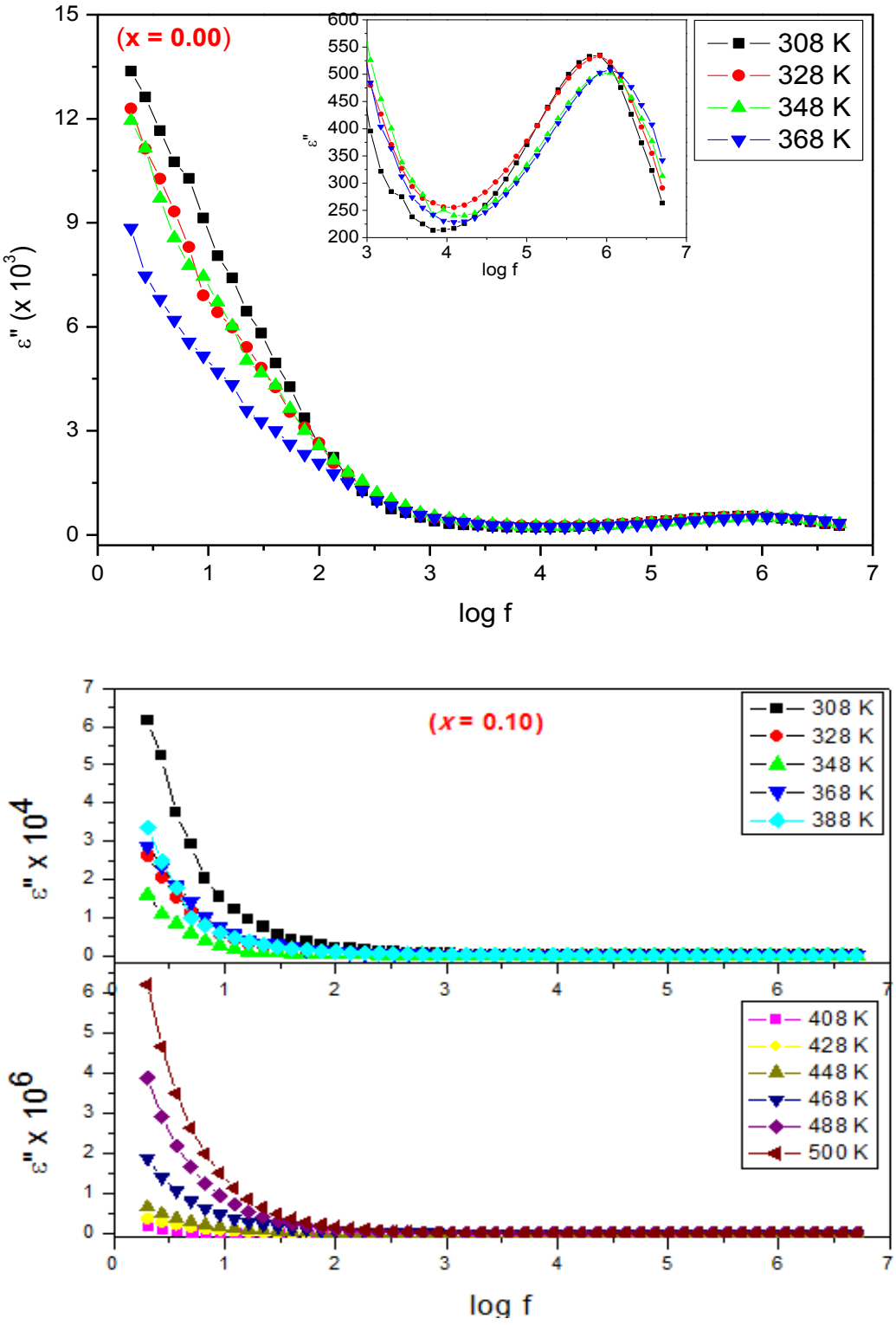

Figure 5.11 (I): Variation of imaginary part of dielectric constant (ε″) with frequency at few selected temperatures for $Y_{2/3}Cu_{3-x}Zn_xTi_4O_{12}$ ceramic (x = 0.00 and 0.10) sintered at 950 °C for 12h.

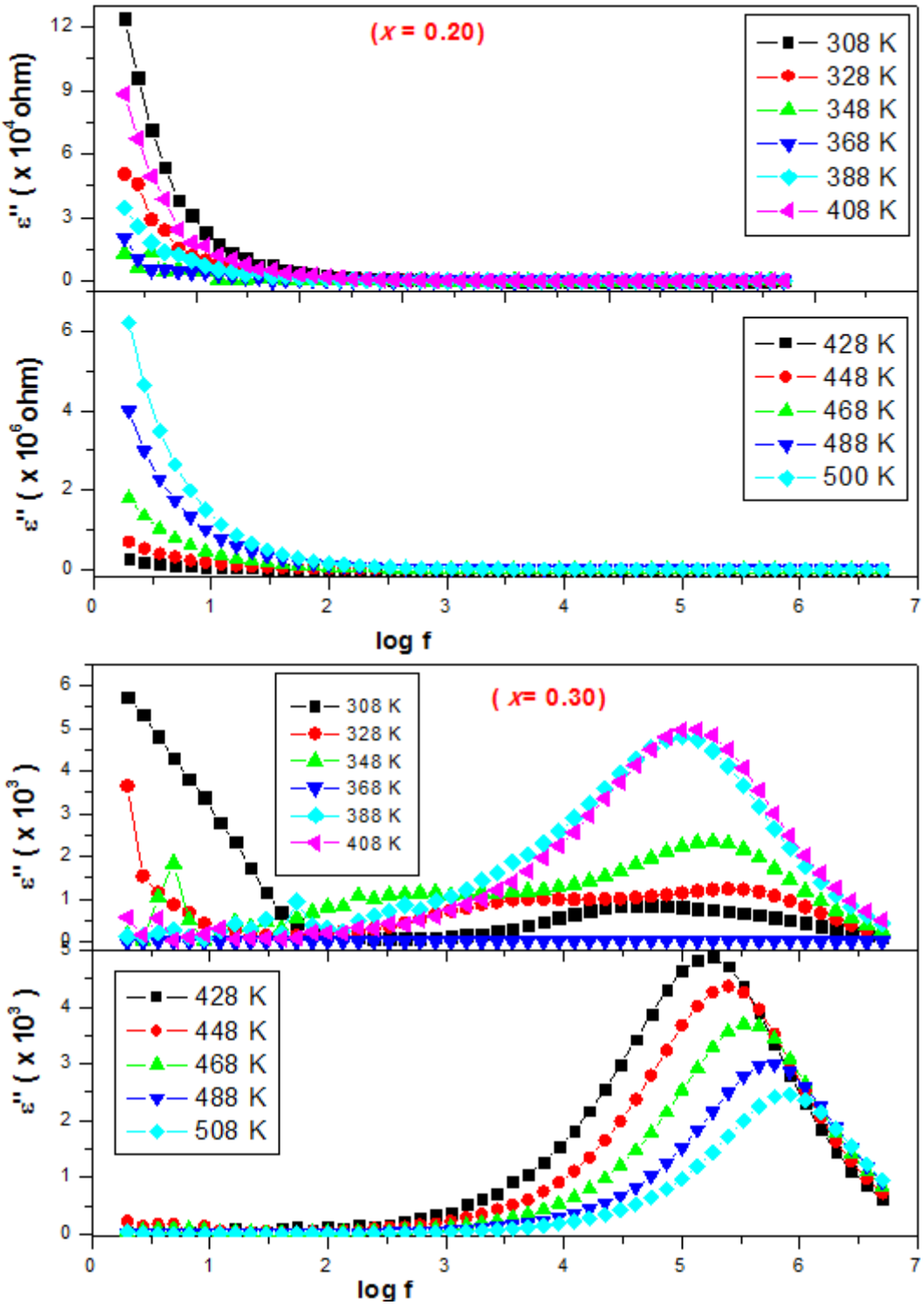

Figure 5.11 (II): Variation of imaginary part of dielectric constant (ε″) with frequency at few selected temperatures for $Y_{2/3}Cu_{3-x}Zn_xTi_4O_{12}$ ceramic (x = 0.20 and 0.30) sintered at 950 °C for 12h.

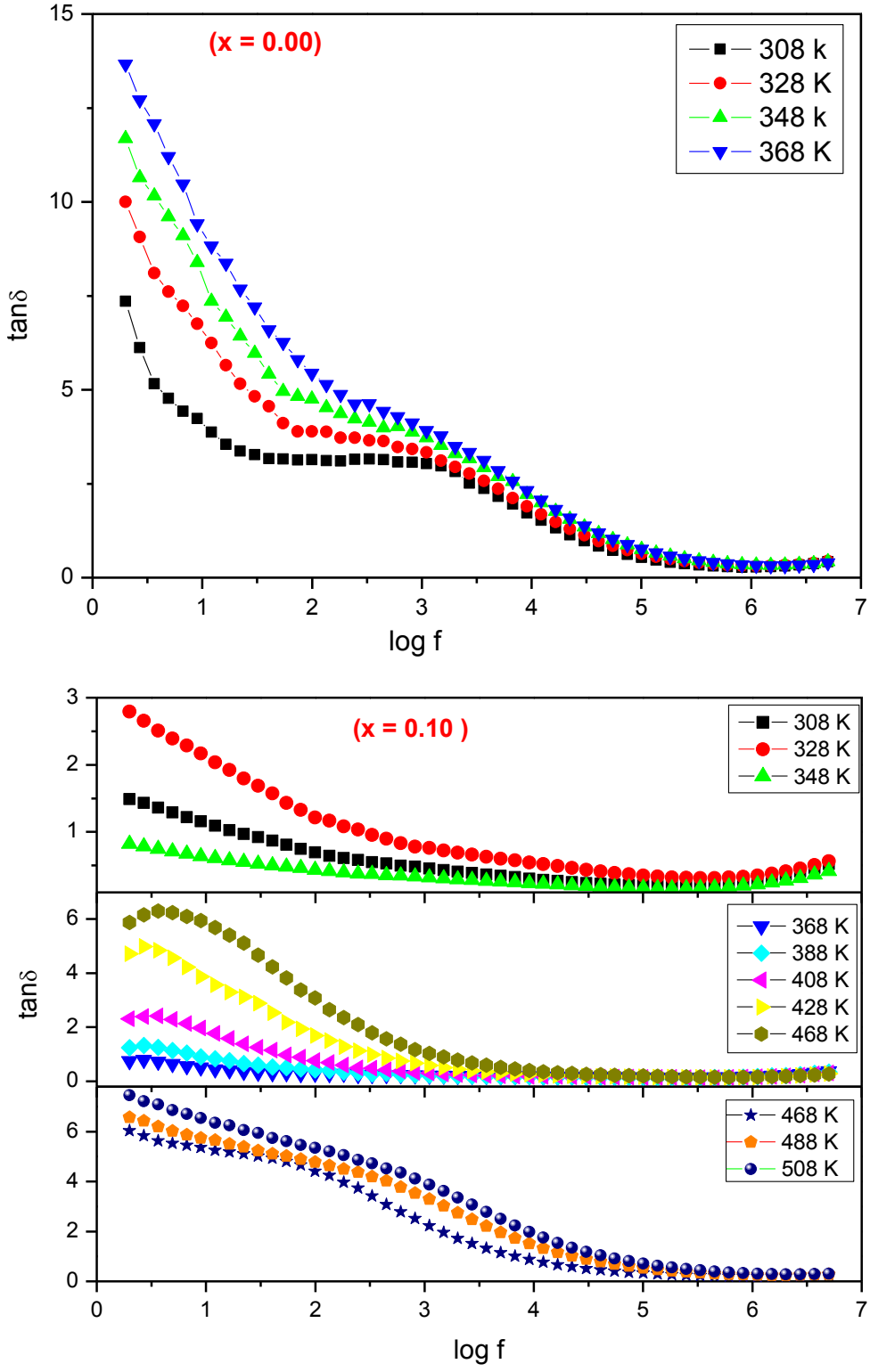

Figure 5.12 (I): Variation of tangent loss (tan δ) with frequency at few selected temperatures for $Y_{2/3}Cu_{3-x}Zn_xTi_4O_{12}$ ceramic (x = 0.00 and 0.10) sintered at 950 $^{\circ}$C for 12h.

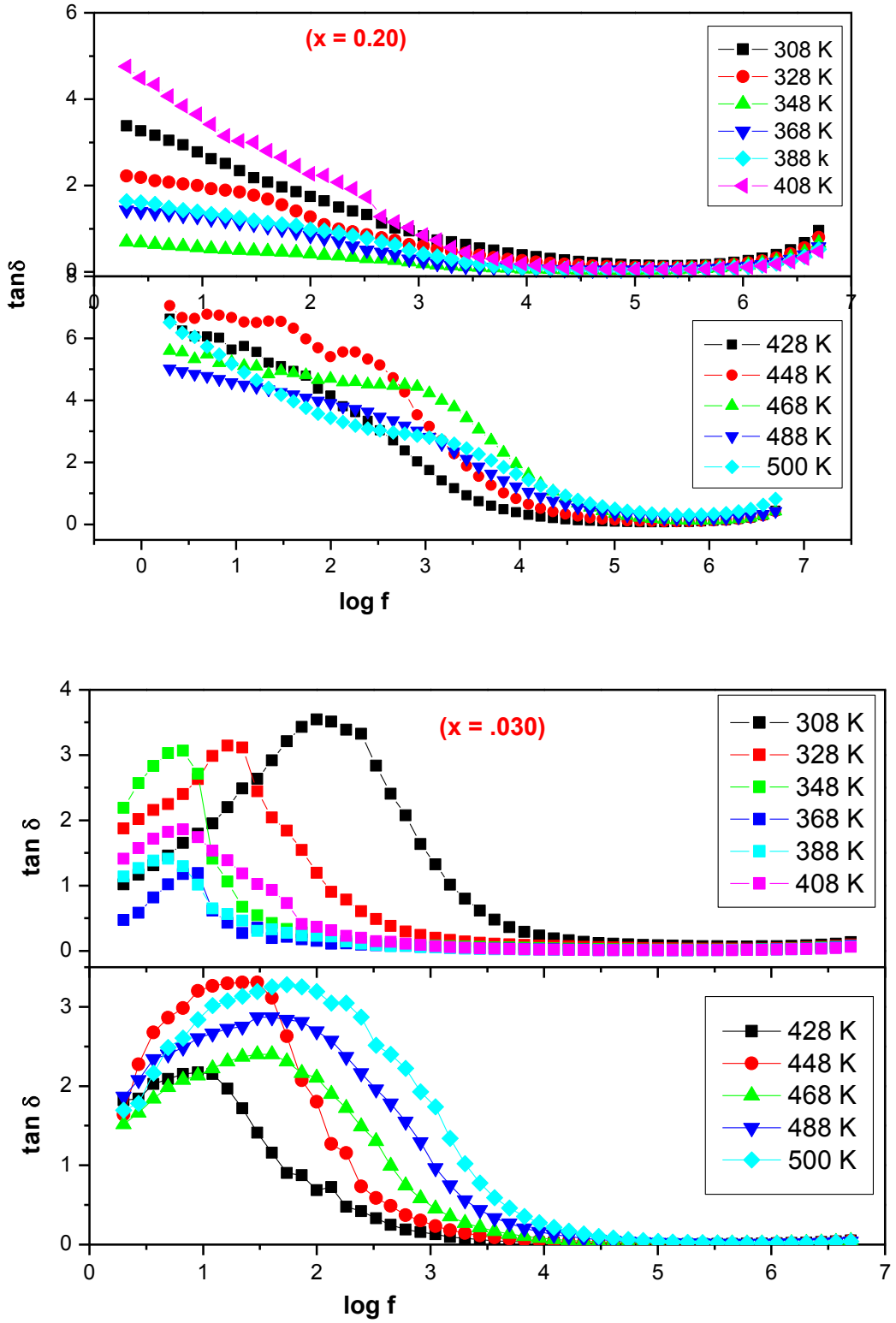

Figure 5.12 (II): Variation of tangent loss (tan δ) with frequency at few selected temperatures for $Y_{2/3}Cu_{3-x}Zn_xTi_4O_{12}$ ceramic (x = 0.20 and 0.30) sintered at 950 $^{\circ}$C for 12h.

The dielectric loss in a low frequency region may be attributed to the conduction of oxygen vacancies originated by mass diffusion during sintering process but slight increases in value of tan δ with frequency may cause due to high conductivity associated with the grain boundary. In such condition the grain boundary becomes insulating. The insulating nature of grain boundary may be attributed to the sintering effects and its conditions. Normally oxygen diffusion takes place during sintering due to the difference in the partial pressure of oxygen in the ceramic oxide and the atmosphere. As grain boundary is associated with a higher diffusion coefficient, the rate of oxygen diffusion is usually more at grain boundary in comparison to grain and in turn, the extent of reoxidation is more at grain boundary during the process of cooling. These above mentioned effects may lead to semiconducting grain and insulating grain boundary in YCZTO ceramic like several oxide ceramic and supporting IBLC mechanism.

5.2.8 Impedance Analysis

The values of resistance (R) and capacitance (C) associated with an electrically active grain and grain boundary regions in the bulk polycrystalline electro-ceramics can be estimated by impedance spectroscopy which correlates electrical behavior of the sample to its microstructure. Complex impedance spectroscopy is a powerful tool in separating out the grain and the grain boundary effects (Hodge *et al.*, 1976). Electrical behaviour of YCZTO ceramic has been characterized over a wide range of frequency and temperature by employing the complex impedance (Z*) to disclose the reasons for dielectric dispersion and formation of barrier layer in YCZTO ceramic as well as presence of multi-polarization processes appearing simultaneously in the ceramic with their usual relaxation conditions. In polycrystalline materials, impedance formalism emphasizes grain boundary conduction effects, while bulk effects get dominated in the electric modulus formalism.

The Nyquist plot between Z' and Z'' of sintered $Y_{2/3}Cu_{3-x}Zn_xTi_4O_{12}$ (x = 0.10) ceramic at a few selected temperature is shown in Fig. 5.13. It is quite clear from the graph that all the curves exhibit a common tendency to bend towards the abscissa to form semicircles with their centers below the real axis. Fig. 5.13 is further characterized by the presence of a single semi-circular arc at 308-500 K.

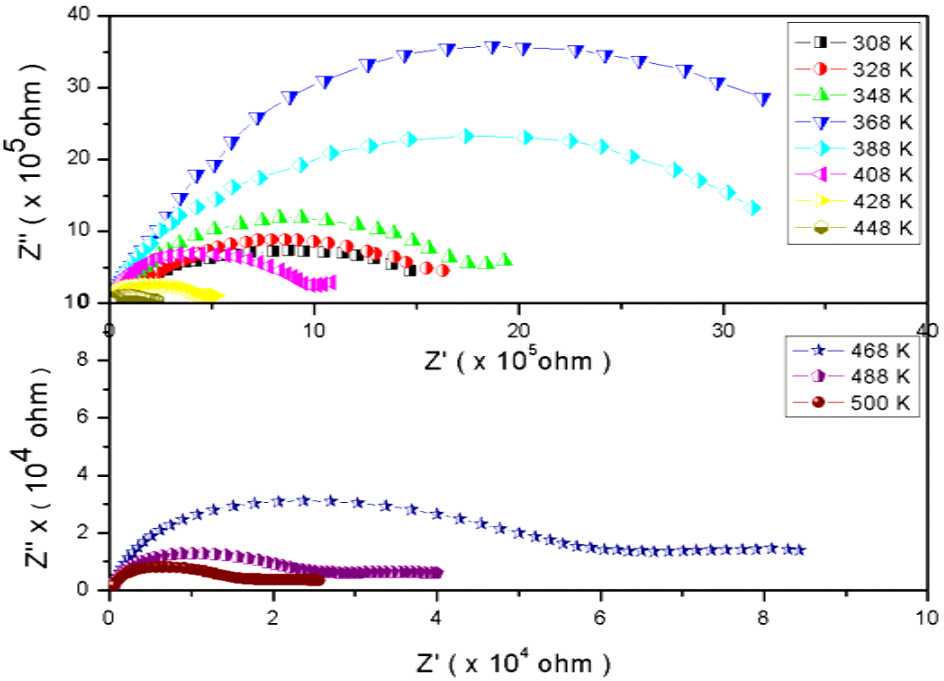

Figure 5.13: Complex impedance plane plots (Z' vs Z'') for $Y_{2/3}Cu_{3-x}Zn_xTi_4O_{12}$ (x = 0.10) ceramic at few selected temperature for sintered YCZTO ceramic.

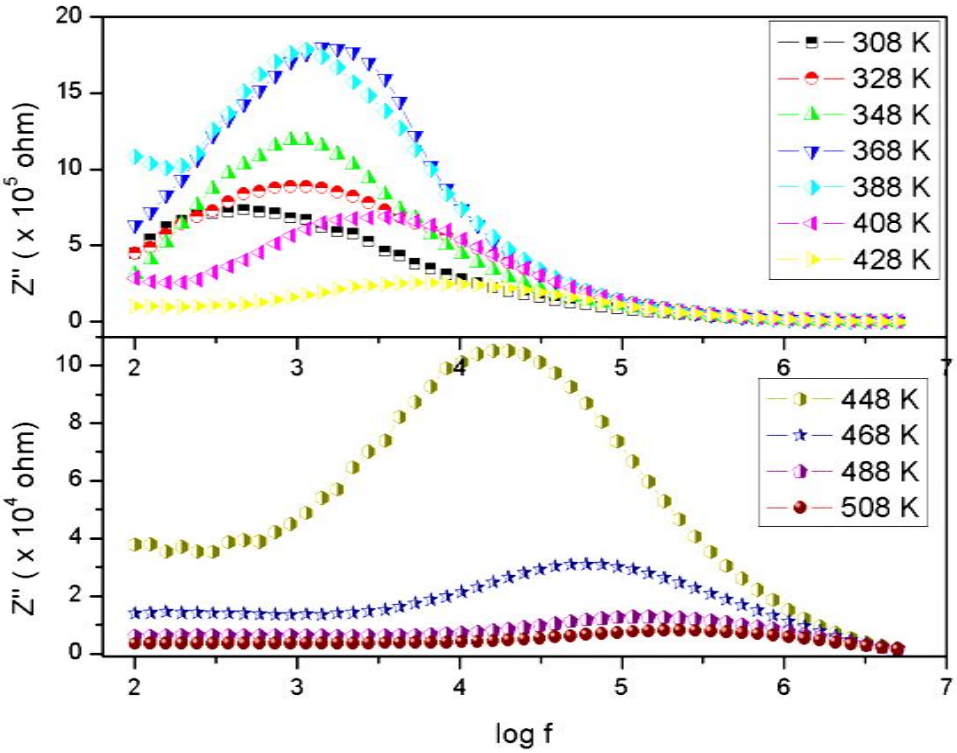

Figure 5.14: Variation of Z'' with frequency for $Y_{2/3}Cu_{3-x}Zn_xTi_4O_{12}$ (x = 0.10) ceramic at few selected temperatures for sintered YCZTO ceramic.

However, in the low frequency region, the complex impedance plot at 468-500 K, neither shows the complete semicircle nor any characteristic electrode spike rather a long residual tail exists. It may be due to the grain boundary or electrode surface effects or both depending upon the temperature. The absence of an electrode-spike indicates that the material is an electronic conductor in the non-ferroelectric orientation at 308-448 K. The semicircular arc corresponding to grain at high frequency has been suppressed due to high value of grain boundary resistance which is analogous to internal barrier layer capacitance (IBLC), characterized by semiconducting grain with insulating grain boundary.

On extrapolation in high frequency region, the intercept on Z′ axis (in Fig 5.13), is not found to be close to zero, suggesting that there must be an existence of another semi-circle in high frequency region beyond the measuring frequency range. The non-zero intercept of the arc passing through the origin on Z′ axis gives the effective contribution of the grain resistance (R_g) value while that of the another arc in the lower frequency range gives contribution of grain boundaries (R_{gb}) to the total resistance. The calculated values of R_g and R_{gb} are listed in Table 5.3.

It is also observed that the radii corresponding to size of different arcs are decreasing with increase in temperature, thereby representing the distribution of relaxation times in the $Y_{2/3}Cu_{3-x}Zn_xTi_4O_{12}$ (x = 0.10) ceramic and indicating a decrease in the resistivity of the material with the increase in temperature. It is also clear from the table that grain boundary resistance decreases with rise in temperature, however, grain resistances do not show much variation with temperature which confirms semiconducting behavior of the grains. From the Table 5.3, it can also be inferred that the resistance of grain boundary is very high in comparison to those of grains which confirms insulating behavior of the grains boundary.

The variation of the imaginary part of impedance Z″ of sintered $Y_{2/3}Cu_{3-x}Zn_xTi_4O_{12}$ (x = 0.10) ceramic with frequency at a few selected temperatures is shown in Fig. 5.14 which shows relaxation peaks at all measured temperatures. The decrease in magnitudes of Z'' with increase in frequency implied that relaxation in YCZTO material is quite temperature-dependent and apparently there is no single relaxation time which implies that there is distribution of relaxation times. A significant broadening of relaxation peaks with a rise in temperature again confirms the existence of a temperature-dependent electrical relaxation phenomenon in the

material. The asymmetric broadening of peaks in YCZTO (x = 0.10) ceramic also suggests the presence of electrical phenomena with a wide spread of relaxation time.

Table 5.3: Calculated values of resistances and capacitances of grain and grain boundary at a few temperatures for sintered $Y_{2/3}Cu_{3-x}Zn_xTi_4O_{12}$ (x = 0.10) nano-ceramic.

Temp. (K)	**R_g(Ω)**	**R_{gb}(Ω)**	**C_g (pF)**	**C_{gb} (nF)**
308	347	1.70×10^6	-	-
328	292	1.84×10^6	-	-
348	296	1.98×10^6	-	-
368	302	4.48×10^6	-	-
388	271	3.52×10^6	-	-
408	271	1.03×10^6	-	5.25
428	239	0.49×10^6	-	4.59
448	241	0.22×10^6	-	4.40
468	206	0.06×10^6	-	4.10
488	122	0.02×10^6	-	-
500	60	0.01×10^6	-	3.80

The factors responsible for relaxation behavior in this ceramic may possibly be the presence of immobile species or electrons at low temperature and defects or vacancies at higher temperature. The localized relaxation which is basically due to defect relaxation, in case of dielectric materials, dominates because of the low dielectric ratio = $\varepsilon_s/\varepsilon_\infty$, where ε_s and ε_∞ are dielectric constants at low and high frequencies, respectively. Dispersion of the resultant curves in the low frequency region at different temperatures is very clear which appears to be merging at higher frequency irrespective of temperature variations in YCZTO (x = 0.10). Such behaviour may be due to the presence of the space charge polarization effects at lower frequency which definitely gets eliminated at higher frequency (Dhawajam *et al.*, 2012).

Furthermore, these peaks get suppressed but slightly shifted to high frequency region on increasing temperature indicating thereby the possible release of space charge accumulation at the boundaries of homogeneous phases in the test material under the applied external field. All these evidences support the existence of a temperature-dependent Maxwell-Wagner dielectric relaxation.

5.2.9 Modulus spectroscopic studies

The presence of long-range conduction phenomenon as well as different types of microscopic processes responsible for localized dielectric relaxations in YCZTO ceramics were investigated separately by modulus spectroscopic studies. Impedance data was re-plotted in modulus formalism to confirm the presence of grain and grain boundary effects. In fact Sinclair and West first suggested the combined usage of impedance and modulus spectroscopic plots to rationalize the dielectric properties.

The temperature dependent Cole-Cole plot between M′ and M″ is shown in Fig. 5.15 which clearly indicates the presence of semicircles for each temperatures (from 308 K-500 K) having their centre below the real axis, suggesting thereby the presence of grain boundaries along with the grains in YCZTO ceramic. The Cole–Cole plot also justifies a poly-dispersive nature for the dielectric relaxation at low frequencies. Such observations may possibly be related to the lack of resorting force governing the mobility of charge carriers under the action of an induced electric field. This behaviour supports the long range mobility of charge carriers.

In order to explain the modulus spectra of YCZTO ceramic, the variation of the imaginary part of electric modulus M″ is plotted against frequency at few selected temperatures and is shown in Fig. 5.16. It clearly exhibits the presence of well-defined relaxation peaks at a few selected temperatures. The presence of relaxation peak in the higher frequency region may be due to grain. The relaxation peaks due to grain and grain boundary responses usually occur at frequencies $1/(2\pi R_g C_g)$ and $1/(2\pi R_{gb} C_{gb})$, respectively. As the peak values are proportional to the reciprocal of the associated capacitance; the smallest capacitance will dominate in the electric modulus plots. The grains usually have smaller capacitances than the grain boundaries; as their peak is stronger in the modulus spectra.

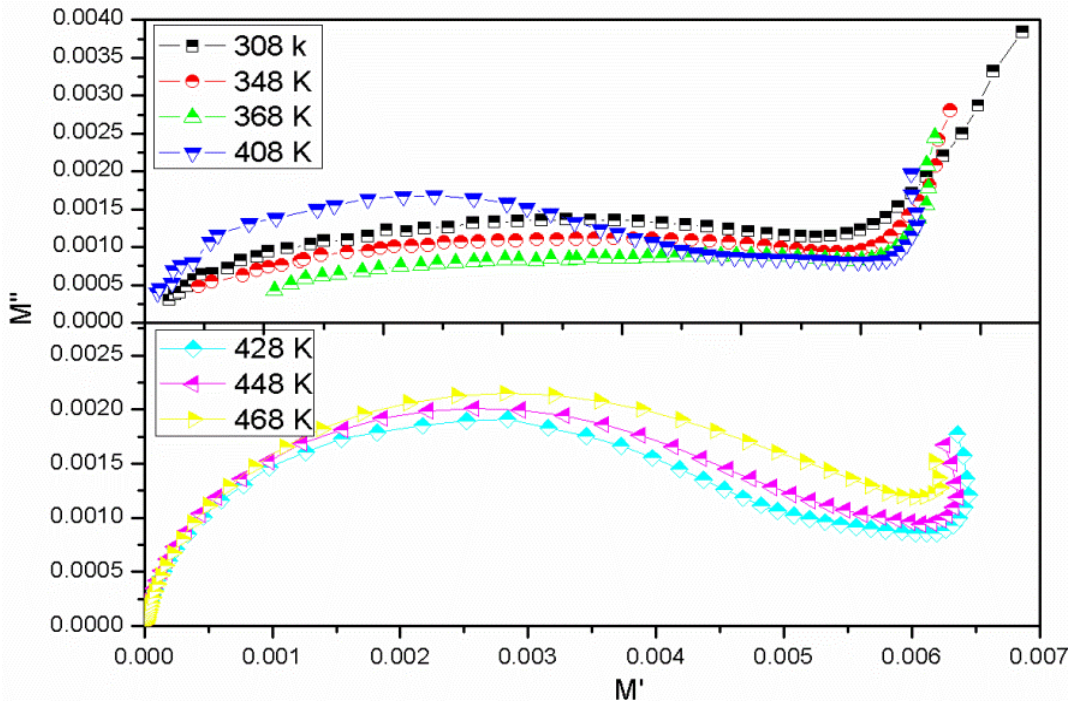

Figure 5.15: Electric modulus plots M′ vs M″ for sintered $Y_{2/3}Cu_{3-x}Zn_xTi_4O_{12}$ (x = 0.10) ceramic at a few selected temperature.

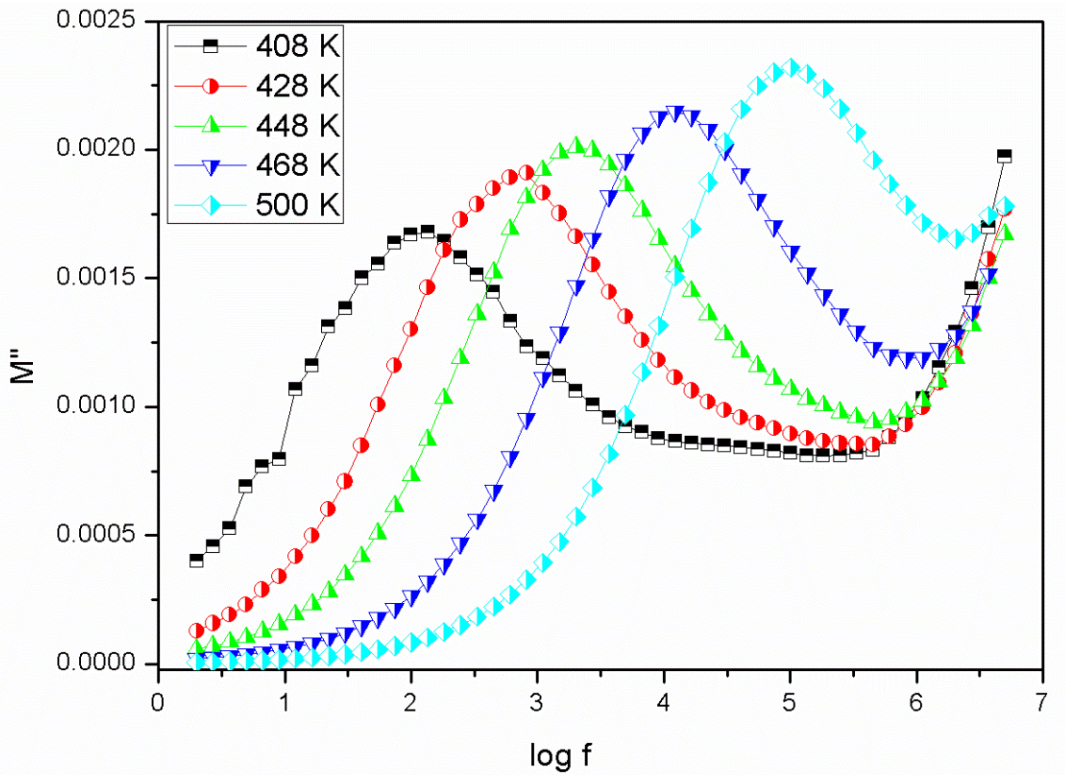

Figure 5.16: Variation of M″ vs frequency for $Y_{2/3}Cu_{3-x}Zn_xTi_4O_{12}$ (x = 0.10) ceramic at a few selected temperatures.

The capacitance of grain boundary were also calculated from the plot and recorded in Table 5.3. It is observed that the height of all the relaxation peaks (Fig. 5.15) didn't remain constant rather keeps on increasing with temperature indicating thereby i.e. capacitance is decreasing.

Furthermore, the frequency region below the relaxation peak determines the range in which charge carriers are mobile on long distances at a particular temperature. At frequencies above f_{max}, the charge carriers are mobile on short distances because they remain confined to their potential wells. Again, the relaxation peaks shift to higher frequency region with increasing temperature and providing a direct evidence for temperature dependent relaxation. This behavior also suggests that the dielectric relaxation is YCZTO ceramic is thermally activated (Dhawajam *et al.*, 2012).

5.3 CONCLUSIONS

Nano-sized $Y_{2/3}Cu_{3-x}Zn_xTi_4O_{12}$ (x = 0.00, 0.10, 0.20 and 0.30) ceramics were synthesized by the semi-wet route and its dielectric properties were studied as a function of frequency and temperature. Single phase formation along with the presence of minor secondary phase of CuO of the ceramic was confirmed by XRD characterization. The crystallite size obtained by TEM studies for different YCZTO ceramics was found to lesser than XRD studies. Microstructure with normal grain growth was observed in YCZTO ceramic. Zinc doping at Cu-site provides a giant dielectric value, which could be attributed to the heterogeneous microstructure of semiconducting grains and insulating grain boundaries. With increasing temperature, the dielectric constant and tangent loss increases. The impedance studies of YCZTO (x = 0.10) ceramic showed two major contributions associated with the grain boundaries and electrode effect. The resistance of grain-boundaries appears as a major contribution at higher temperature and electrode resistance appear at low temperature due to electrode polarization. The asymmetric broadening of peaks in YCZTO (x = 0.10) ceramic also suggests the presence of electrical phenomena with a wide spread of relaxation time. Impedance and Modulus analysis of YCZTO (x = 0.10) ceramic, both, confirmed the presence of temperature dependent Maxwell-Wagner type of relaxation.